

High resolution image reconstruction with constrained, total-variation minimization

Emil Y. Sidky, Rick Chartrand, *Member, IEEE* Yuval Duchin, Christer Ullberg, *Member, IEEE*
and Xiaochuan Pan, *Fellow, IEEE*

Abstract—This work is concerned with applying iterative image reconstruction, based on constrained total-variation minimization, to low-intensity X-ray CT systems that have a high sampling rate. Such systems pose a challenge for iterative image reconstruction, because a very fine image grid is needed to realize the resolution inherent in such scanners. These image arrays lead to under-determined imaging models whose inversion is unstable and can result in undesirable artifacts and noise patterns. There are many possibilities to stabilize the imaging model, and this work proposes a method which may have an advantage in terms of algorithm efficiency. The proposed method introduces additional constraints in the optimization problem; these constraints set to zero high spatial frequency components which are beyond the sensing capability of the detector. The method is demonstrated with an actual CT data set and compared with another method based on projection up-sampling.

I. INTRODUCTION

THIS proceedings focuses on a fundamental issue of resolution in iterative image reconstruction (IIR). IIR is being considered for application in computed tomography (CT), see for example [1], because it is possible to account for noise in the data model and accordingly allow for high quality images with a reduced exposure [2]. IIR methods being considered for CT, all involve implicit solution, see section 15.3 of [3], for the image as opposed to explicit solution, derived from exact or approximate inverses to the continuous cone-beam transform. For explicit reconstruction algorithms, which are generally some variant of filtered back-projection (FBP), the reconstructed volume can be obtained one point at a time. Images can be shown on grids of any size and with arbitrarily small grid spacing, for example blowing up a region-of-interest (ROI). Note, that does not mean the resolution is arbitrarily high, because the system resolution is still limited by the discrete data sampling. Reconstruction by implicit solution allows more flexible and realistic data models for the tomographic system, but at a price. As pointed out often, IIR algorithms are generally more computationally intensive. Another important issue is that a complete expansion

set for the imaged volume is necessary in order to obtain the reconstruction, and the complete image must be solved for all at once; the image cannot be gotten voxel-by-voxel.

More concretely, let us consider a linear imaging model using a voxel expansion of the volume and ideal conditions of perfect data consistency:

$$\mathbf{g} = \mathcal{X}\mathbf{f}, \quad (1)$$

where \mathbf{g} represents the projection data as a 1D vector; \mathbf{f} is a vector of voxel values; \mathcal{X} is the system matrix, which yields line integrals through the volume and for the present work is based on the ray intersection length as specified in Siddon's method. This model, which forms the basis of many IIR algorithms, is difficult to solve explicitly for realistic size models of a CT system. The matrix \mathcal{X} is ill-conditioned and can be extremely large, up to a size of $10^9 \times 10^9$. Equation (1) is usually solved implicitly by one of many algorithms, conjugate gradients, algebraic reconstruction techniques (ART), etc. Two practical issues arise in the implicit solution of Eq. (1): (I) the voxel representation of the image must include the whole region where the measured transmission rays intersect with the support of the subject [4], and (II) to attain the intrinsic resolution of the data the voxels must be small compared with the detector bin width. The combination of these two factors causes a computational burden, because straight-forward voxelization of the reconstruction volume will lead to a very large array. But also, mathematically, the second point that voxels should be small compared to the detector bins leads to an under-determined linear system for Eq. (1), because there will be more unknown voxel values than known ray-transmission measurements. In this work, we examine a couple of possible solutions for addressing the second issue – dealing with the large null-space of Eq. (1) in a controlled way.

In Sec. II we present the image reconstruction algorithms and in Sec. III we demonstrate them on an actual low-intensity CT scan.

II. CONSTRAINED, TOTAL-VARIATION MINIMIZATION THEORY AND ALGORITHMS

In recent years, we have been investigating the solution of Eq. (1), by solving the constrained TV-minimization problem:

$$\mathbf{f}^* = \operatorname{argmin} \|\mathbf{f}\|_{\text{TV}} \text{ such that } |\mathcal{X}\mathbf{f} - \mathbf{g}|^2 \leq \epsilon^2 \quad \mathbf{f} \geq 0, \quad (2)$$

where $\|\mathbf{f}\|_{\text{TV}}$ is the sum over the gradient magnitude image; and ϵ is a data-error tolerance parameter necessary because the

Manuscript received November 21, 2010. This work was supported in part by NIH R01 grants CA120540 and EB000225. The contents of this article are solely the responsibility of the authors and do not necessarily represent the official views of the National Institutes of Health. This work was also supported in part by the U.S. Department of Energy through the LANL/LDRD Program.

E. Y. Sidky, Y. Duchin, and X. Pan are with the University of Chicago Dept. of Radiology, Chicago, IL 60637 USA.

R. Chartrand is with Los Alamos National Laboratory, Los Alamos, NM 87545 USA.

C. Ullberg is with XCounter AB, Danderyd, SE-182 33 Sweden.

projection data is likely not consistent with the image model. To solve this optimization problem, we have been developing a heuristic algorithm [5], [6], [7], [8], [9], [10] that alternates between projection-onto-convex-sets (POCS), to enforce the constraints, and steepest descent (SD) to reduce image TV. The key point of this algorithm is that the SD step-size is controlled adaptively, so as to not undo progress toward the feasible image set with POCS. This alternating algorithm is called adaptive SD-POCS (ASD-POCS). For investigations where solving Eq. (2) accurately is important, optimality conditions should be checked [6], [10]. On the other hand, for practical applications it may not be necessary to have an accurate solver [7], and in such cases ASD-POCS yields a clinically useful image within 10-20 iterations.

Image reconstruction algorithms for CT based on Eq. (2) have been shown to be effective for sparse-view projection data [5], [11], [12], [6], [7], [13], [9], [14], [15], [16], which has obvious implications for patient dose. More recently, we have been interested in how to apply ASD-POCS to what has traditionally accepted as fully angularly-sampled data. For such data, structures on the scale of a detector bin-width are expected to be resolved. For IIR, this requirement poses the above-mentioned problem that the number of voxels may be much larger than the number of data, and direct application of the IIR algorithm may lead to strange noise patterns which can interfere with imaging tasks [10]. There are likely many ways to resolve this problem; for example, introducing a non-zero cross-section to the ray model in \mathcal{X} may yield nicer noise patterns while maintaining image resolution. At the same time, more realistic system model ling usually comes at the expense of computational speed. As a result, we have been seeking other alternatives.

In Ref. [10], we propose to stabilize the problem in Eq. (2) by making the following observation: CT resolution is non-uniform, and generally, the angular-sampling is worse than detector resolution. Assuming that the individual projection sampling satisfies Nyquist frequency, each projection can be up-sampled to increase the number of measurement rays at each projection. We will still have a data set which is under-sampled in the angular direction with respect to the very high resolution imaging grid. But we already know that TV-minimization approaches appear to be effective with this type of under-sampling. We refer to this approach as up-sampling ASD-POCS or, in this text, as simply up-sampling.

In this proceedings, we propose another approach which may have even a greater advantage in terms of algorithm efficiency. The method comes from realizing that while we need many voxels per bin-width for flexibility of the image representation, we cannot hope to actually attain true super-resolution where structures smaller than the detector bin are visible. To capture this idea mathematically, we impose constraints on the Fourier transform of the image. Specifically, high frequency components of the image are set to zero:

$$\mathcal{F}(|\nu| > \nu_{\max}) = 0, \quad (3)$$

where \mathcal{F} is the discrete Fourier transform (DFT); ν represents spatial frequency; and the frequency magnitude ν_{\max} is determined by the bin spacing. If the detector bins have width w , we

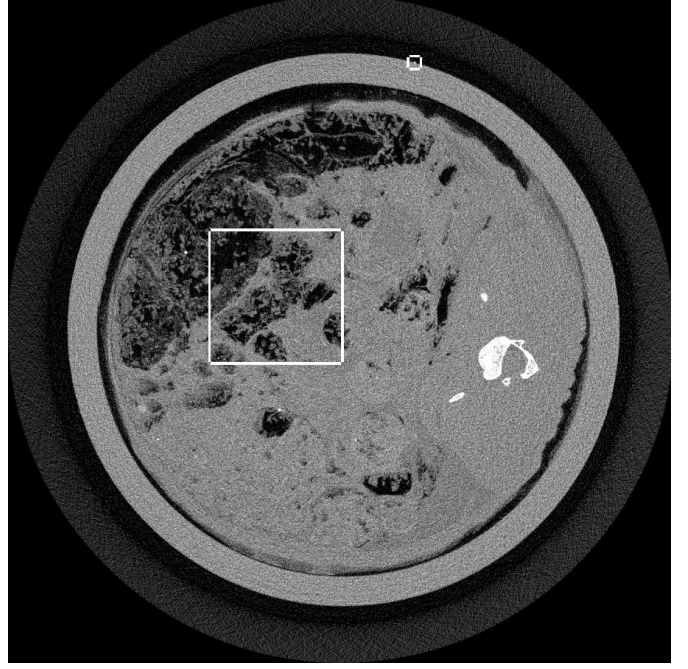


Fig. 1. FBP slice image of a rabbit scanned by a low-dose XCounter CT system. The raw FBP image was smoothed by a Gaussian filter, reducing the image TV by a factor of 8. The indicated rectangles show the ROIs which are used for the algorithm comparisons. In particular, the small one surrounds the wire object used to obtain a sense of resolution. The display window is $[0, 0.04] \text{ mm}^{-1}$.

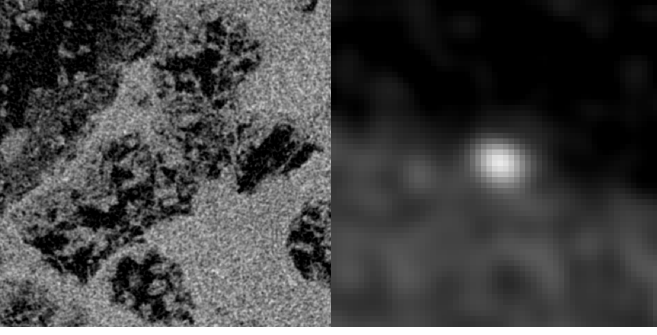
set $\nu_{\max} = 1/(2\pi w)$. Although this choice makes sense physically, ν_{\max} can be taken as a algorithm parameter, but varying ν_{\max} is beyond the scope of this study. Adding this constraint to the optimization problem in Eq. (2) leads to frequency-constrained ASD-POCS. This approach involves processing fewer data in exchange for computing DFTs, which can be done efficiently with the fast Fourier transform. The pseudo-code for frequency-constrained ASD-POCS is the same as that reported in Ref. ([10]) with the additional steps of enforcing Eq. (3) at each line where the image positivity is enforced. For the present results, the frequency constraint was imposed before positivity.

III. RESULTS

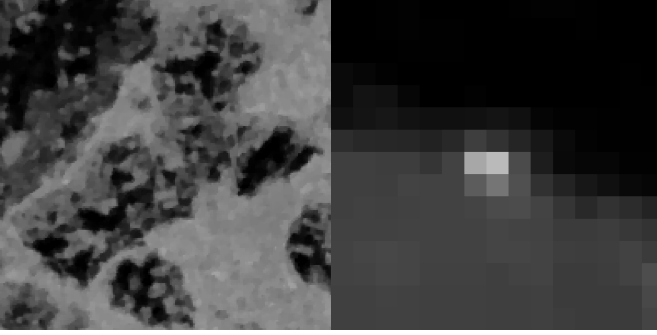
The up-sampling and frequency constrained ASD-POCS algorithms are demonstrated with an XCounter CT scan of a rabbit with a thin wire taped to the outside of the sample holder. The data are low-intensity and contain 1878 projections with a 2266×64 bin detector at a resolution of 0.1 mm. The thin wire provides a good resolution test for the image reconstruction algorithm. For the present purpose, we take the middle row on the detector from this data set and focus on 2D fan-beam CT reconstruction with 1878 projections on a 2266-bin linear detector array.

An FBP image of this data set is shown in Fig. 1, where some regularization is performed by Gaussian smoothing with a window 2 pixels wide. The rectangles indicate the regions where comparisons of the different algorithms are shown. Comparisons for each algorithm will be made at a level of image regularization where each image's TV-norm is an eighth

Gaussian-filtered FBP



ASD-POCS (0.1 mm pixels)



ASD-POCS (0.025 mm pixels)

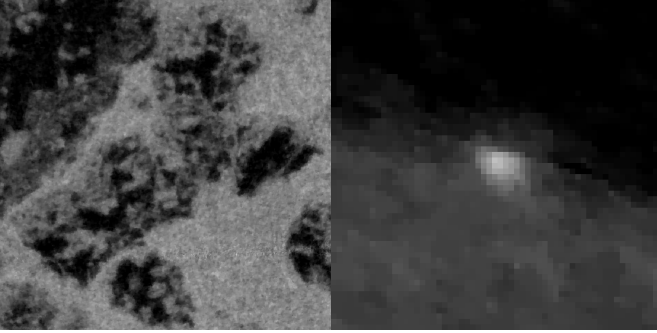
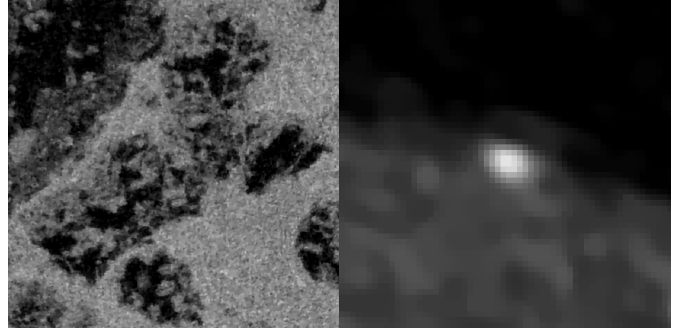


Fig. 2. (Top) FBP ROI's for the image presented in Fig. 1. (Middle) ASD-POCS image reconstructed from original data for a grid with 0.1 mm pixels. (Bottom) ASD-POCS image reconstructed from original data for a grid with 0.025 mm pixels. The image TV for each case is set to an eighth of that of the raw FBP image. The display window is $[0, 0.04] \text{ mm}^{-1}$ on the left ROI and $[0, 0.09] \text{ mm}^{-1}$ on the right ROI.

of that of the unregularized FBP image. The images are shown just to give a sense about the behavior of the algorithms; more rigorous evaluation with different levels of regularization will be performed in future work.

We illustrate the problems with employing a matched-resolution grid, 1024×1024 , and a very high resolution grid, 4096×4096 , with the basic ASD-POCS algorithm. The pixel width is 0.1 mm for the former grid and 0.025 mm for the latter. Note that the rabbit support projects onto the middle 1000 bins of the full projection. The FBP image is shown on a 4096×4096 grid, but because FBP is based on an explicit inverse its pixel values are not affected by the grid size. In Fig. 2 the matched grid clearly leads to a loss of resolution

ASD-POCS (projection up-sampling)



ASD-POCS (spatial frequency constraints)

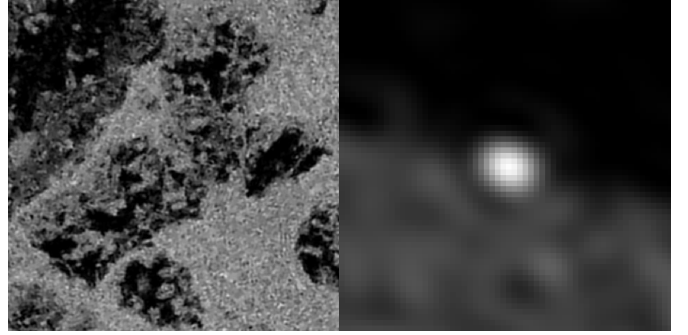


Fig. 3. (Top) ASD-POCS image obtained from the up-sampled data set. (Bottom) ASD-POCS image reconstructed from original data set with additional constraints on the spatial frequency. For both images the pixel width is 0.025 mm. The image TV for each case is set to an eighth of that of the raw FBP image. The display window is the same as that of Fig. 2

relative to FBP, because the image is forced to be uniform over the $0.1 \text{ mm} \times 0.1 \text{ mm}$ squares. Simply going to a larger array does improve the ASD-POCS image, but the noise pattern shows additional false structure when compared with the FBP image. These structures arise from the fact that the imaging problem is under-sampled by roughly a factor of ten and this under-sampling occurs in both view-angle and detector-bin directions. The random, sparse specks that appear could be confused with micro-calcifications in the context of breast imaging.

Finally, we show images for ASD-POCS using up-sampling and frequency constraints, and the resulting region-of-interest images are shown in Fig. 3. For the up-sampling method the data are up-sampled at each projection so that the data set size nominally becomes 1878 views by 9064 virtual bins prior to reconstruction by ASD-POCS. The frequency constraint ASD-POCS takes the original 1878×2266 data set as input. As can be seen in the figure, both approaches remove the disturbing noise pattern seen at the bottom of Fig. 2. Each of these images show some potential advantage over FBP in that the wire appears to be better focused in the up-sampling approach, and the image noise level is reduced approximately 20% for both up-sampling and frequency constrained ASD-POCS. It is possible that the frequency constraint method could lead to better resolution by allowing ν_{\max} to be increased. Such a study will be investigated in future work.

IV. CONCLUSION

We have developed modifications to ASD-POCS that allow for high-resolution recovery of structures occurring on the scale of the detector bin width. In particular, in this work we show that including constraints on the spatial frequencies of the reconstructed image can improve ASD-POCS images by eliminating false structures, which arise from the large null-space inherent in the imaging model when very high-resolution grids are used to represent the image. Further research, will compare the up-sampling and frequency constraint approaches with many data sets and different levels of image regularity, and we will also look into implementing more realistic ray-models that account for source spot-size and the extent of the detector bins. This realistic modeling in conjunction with frequency extrapolation [17] may allow even further improvement of CT image quality.

REFERENCES

- [1] A. C. Silva, H. J. Lawder, A. Hara, J. Kujak, and W. Pavlicek, "Innovations in ct dose reduction strategy: Application of the adaptive statistical iterative reconstruction algorithm," *Am. J. Roent.*, vol. 194, pp. 191–199, 2010.
- [2] C. H. McCollough, A. N. Primak, N. Braun, J. Kofler, L. Yu, and J. Christner, "Strategies for reducing radiation dose in ct," *Radiol. Clin. N. Am.*, vol. 47, pp. 27–40, 2009.
- [3] H. H. Barrett and K. J. Myers, *Foundations of Image Science*. Hoboken, NJ: John Wiley & Sons, 2004.
- [4] A. Ziegler, T. Nielsen, and M. Grass, "Iterative reconstruction of a region of interest for transmission tomography," *Med. Phys.*, vol. 35, pp. 1317–1327, 2008.
- [5] E. Y. Sidky, C.-M. Kao, and X. Pan, "Accurate image reconstruction from few-views and limited-angle data in divergent-beam CT," *J. X-ray Sci. Tech.*, vol. 14, pp. 119–139, 2006.
- [6] E. Y. Sidky and X. Pan, "Image reconstruction in circular cone-beam computed tomography by constrained, total-variation minimization," *Phys. Med. Biol.*, vol. 53, pp. 4777–4807, 2008.
- [7] E. Y. Sidky, X. Pan, I. S. Reiser, R. M. Nishikawa, R. H. Moore, and D. B. Kopans, "Enhanced imaging of microcalcifications in digital breast tomosynthesis through improved image-reconstruction algorithms," *Med. Phys.*, vol. 36, pp. 4920–4932, 2009.
- [8] X. Pan, E. Y. Sidky, and M. Vannier, "Why do commercial CT scanners still employ traditional, filtered back-projection for image reconstruction?" *Inv. Prob.*, vol. 25, pp. 123 009–(1–36), 2009.
- [9] E. Y. Sidky, M. A. Anastasio, and X. Pan, "Image reconstruction exploiting object sparsity in boundary-enhanced x-ray phase-contrast tomography," *Opt. Express*, vol. 18, pp. 10 404–10 422, 2010.
- [10] E. Y. Sidky, Y. Duchin, C. Ullberg, and X. Pan, "A constrained, total-variation minimization algorithm for low-intensity x-ray CT," <http://arxiv.org/abs/1011.4630>, 2011, accepted to *Med. Phys.*
- [11] J. Song, Q. H. Liu, G. A. Johnson, and C. T. Badea, "Sparseness prior based iterative image reconstruction for retrospectively gated cardiac micro-CT," *Med. Phys.*, vol. 34, pp. 4476–4483, 2007.
- [12] G. H. Chen, J. Tang, and S. Leng, "Prior image constrained compressed sensing (PICCS): a method to accurately reconstruct dynamic CT images from highly undersampled projection data sets," *Med. Phys.*, vol. 35, pp. 660–663, 2008.
- [13] X. Jia, Y. Lou, R. Li, W. Y. Song, and S. B. Jiang, "GPU-based fast cone beam CT reconstruction from undersampled and noisy projection data via total variation," *Med. Phys.*, vol. 37, p. 1757, 2010.
- [14] F. Bergner, T. Berkus, M. Oelhafen, P. Kunz, T. Pan, R. Grimmer, L. Ritschl, and M. Kachelriess, "An investigation of 4D cone-beam CT algorithms for slowly rotating scanners," *Med. Phys.*, vol. 37, pp. 5044–5054, 2010.
- [15] K. Choi, J. Wang, L. Zhu, T.-S. Suh, S. Boyd, and L. Xing, "Compressed sensing based cone-beam computed tomography reconstruction with a first-order method," *Med. Phys.*, vol. 37, pp. 5113–5125, 2010.
- [16] J. Bian, J. H. Siewerdsen, X. Han, E. Y. Sidky, J. L. Prince, C. A. Pelizzari, and X. Pan, "Evaluation of sparse-view reconstruction from flat-panel-detector cone-beam CT," *Phys. Med. Biol.*, vol. 55, pp. 6575–6599, 2010.
- [17] R. Chartrand, E. Y. Sidky, and X. Pan, "Frequency extrapolation by nonconvex compressive sensing," <http://math.lanl.gov/Research/Publications/Docs/chartrand-2011-frequency.pdf>, 2011, accepted to IEEE ISBI.